Generation of CW mid-infrared radiation in the mW power range and tuneable over 400 nm

Riccardo Brameri, Valerio Vitali, Ludovic Gauthier-Manuel, Cosimo Lacava, Federico Pirzio, Antoniangelo Agnesi, Mathieu Chauvet, Ilaria Cristiani

Research Article Vol. 33, No. 3 / 10 Feb 2025 / Optics Express 3759
Optics EXPRESS

Generation of CW mid-infrared radiation in the mW power range and tuneable over 400 nm

Riccardo Brameri,[1,*] Valerio Vitali,[1] Ludovic Gauthier-Manuel,[2] Cosimo Lacava,[1] Federico Pirzio,[1] Antoniangelo Agnesi,[1] Mathieu Chauvet,[2] and Ilaria Cristiani[1]

[1]Department of Electrical, Computer and Biomedical Engineering, University of Pavia, Pavia 27100, Italy
[2]FEMTO-ST institute, UMR CNRS 6174, University of Franche-Comté, 15B Avenue des Montboucons, 25030 Besançon, France
[*]riccardo.brameri01@universitadipavia.it

Abstract: Miniaturization of mid-infrared (MIR) spectroscopy sources has progressed significantly during the past two decades, but a solution able to provide full integration, high optical power and wide tuneability in the so-called atmospheric window (2.5 - 5 µm) is still missing. In this context, we investigated a broadband frequency-tuneable source relying on difference frequency generation (DFG) in a periodically poled lithium niobate (PPLN) ridge waveguide. By employing tuneable lasers for the pump and signal wavelengths emitting at around 1 µm and 1.55 µm, respectively, we were able to fully cover the ≈ 3 - 3.5 µm spectrum, thus translating the technological maturity of data communication photonic sources to the MIR wavelength band. Moreover, the use of a relatively large cross-section for the here-proposed PPLN ridge waveguide compared to commonly employed thin-film lithium niobate (TFLN) waveguides has allowed us to achieve low propagation and coupling losses together with high damage threshold, thereby allowing us to reach mW-level power in the MIR wavelength band.

1. Introduction

Mid-infrared (MIR) optical sensors based on spectroscopy represent powerful tools in several applications, such as environmental monitoring, industrial process control and petrochemical industry [1,2]. The ability to accurately identify different chemical species requires the use of laser sources with spectral lines in the kHz range, output powers of several mW, and fine tuneability in frequency over an extended band of the order of several tens of nm. In particular, the so-called atmospheric window that ranges from 2.5 to 5 µm is of high interest as it contains the spectral fingerprints of several pollutants, such as N_2O, CO_2, NO_2, HCl, NH_3, C_2H_6 and others. The availability of a widely tuneable and powerful MIR source suitable for integration on a photonic integrated circuit (PIC) platform and for mass production is still missing and would represent a revolutionary opportunity in this rapidly expanding application area. Important technological advances for MIR spectroscopy have been the development of room-temperature quantum cascade lasers (QCL) [3–5] and interband cascade lasers (ICL) [6,7], which have extended the operating range of tuneable semiconductor lasers from the visible and near-infrared (NIR) to the MIR. With these sources, a novel generation of sensors suitable for real-time in situ detection of gases is now available. However, such tools, which rely on the assembly of discrete optical components, still fail to meet some key requirements for many applications. The first limitation is related to their limited tuneability, which usually limits their application to the detection of a single species for a given laser source.

#541639 https://doi.org/10.1364/OE.541639
Journal © 2025 Received 25 Sep 2024; revised 5 Nov 2024; accepted 7 Nov 2024; published 27 Jan 2025

Optics EXPRESS

In the present scenario, the exploitation of efficient nonlinear integrated photonic platforms could represent an appealing solution for MIR light generation and amplification with a very compact footprint [8,9]. Indeed, the exploitation of nonlinear processes could allow to efficiently translate the radiation emitted by mature and low-cost telecom optical sources, with excellent linewidth properties, modulation capabilities and wide tuneability, to the MIR spectral region.

Lithium Niobate (LN) is one of the most mature material platforms for the realization of second-order nonlinearity-based integrated photonic devices [10,11]. In recent years, a few results have been reported on the generation of continuous wave (CW) and tuneable MIR radiation exploiting LN-on-insulator (LNoI) platforms. Nonlinear waveguides usually rely on ridge structures obtained by dry etching a very thin LN core layer (typically 300 - 900 nm thick [12–14]) bonded on top of a silica cladding. Such geometry allows obtaining strong modal confinement devices, which were not available in the past; this fuelled a significant research activity based on the exploitation of the LNoI platform for nonlinear applications. The strong modal confinement and flexibility in the waveguide geometry and cladding materials offered by the LNoI platform guarantees new degrees of freedom in tailoring waveguide dispersion, enabling both frequency generation over an ultra-wide bandwidth [15] and intermodal phase matching for multi-wavelength generation in a single waveguide [16]. Despite its outstanding efficiency and versatility, the LNoI platform suffers from some fundamental limitations. Indeed, the typically strong modal mismatch between focused input beams and LNoI waveguide modes at the integrated chip facet commonly results in a very poor butt-coupling efficiency of pump and signal. Typical reported values are in the order of ~1 – 2% [17], which makes this factor relevant when considering the nonlinear performance of the system [18]. In principle, better coupling efficiency can be obtained by the exploitation of grating or edge couplers with advanced designs at the expense of an increased complexity in the waveguide fabrication and a limitation in the operational bandwidth. Moreover, huge field intensities result from the extreme mode confinement in the LNoI waveguides (mode effective area = 0.2 - 1.5 μm^2), which allows achieving very high nonlinear efficiencies. However, absolute values of the MIR output power in the order of a few tens of μW are typically reported, which are insufficient for most spectroscopy applications. In this work, we demonstrate the generation of MIR radiation through difference frequency generation (DFG) tuneable from 3 to 3.5 μm with output power in the mW range. This result is obtained by exploiting a nonlinear LNoI platform based on a ridge waveguide with a cross-section enabling optimal coupling efficiency and low propagation losses for the wavelengths involved in the nonlinear process. This ridge structure consists of a periodically poled LN crystal that guarantees phase-matched interactions over a band exceeding 400 nm. We believe that the proposed device can represent a significant breakthrough towards the development of integrated CW sources able to provide high-power and tuneable radiation in the MIR range for spectroscopy applications.

2. Design and simulations

The proposed device is based on the use of the DFG process exploiting the high second-order nonlinear coefficient d_{33} (25.2 pm/V) of LN. Considering a pump wave at a wavelength λ_p and a signal at a wavelength λ_s, the wavelength λ_i of the generated radiation (idler) is obtained according to the energy conservation principle:

$$\frac{1}{\lambda_i} = \frac{1}{\lambda_p} - \frac{1}{\lambda_s} \tag{1}$$

By considering a pump wavelength λ_p ranging from 1 to 1.1 μm and a signal tuneable in the optical communication C-band (1.53 - 1.565 μm), a MIR radiation in the range from 2.75 to 3.91 μm could be generated. The efficiency of the nonlinear process is mainly dictated by the phase matching (PM) condition that has to be fulfilled between the interacting fields. As already

Optics EXPRESS

extensively reported in the literature, such a condition can be satisfied by periodically poling the ferroelectric domains of the LN waveguide. In this case, the phase-matching condition can be written as [19]:

$$\Delta\beta = \beta_p - \beta_s - \beta_i - \frac{2\pi}{\Lambda} \approx 0, \text{ with } \beta_j = \frac{2\pi n_{eff,j}}{\lambda_j}, \tag{2}$$

where $\Delta\beta$ is the phase-mismatch term, β_j is the propagation constant of the fundamental TM_{00} mode employed in this work at the pump (p), signal (s) and idler (i) wavelengths, $n_{eff,j}$ is the effective refractive index, λ is the wavelength and Λ is the poling period selected to achieve the phase-matching. The designed ridge waveguides exhibited a cross-section of 7×9.6 μm^2 and was 3 cm-long. Since the inversion of the ferroelectric domains is induced by placing a mask on top of the LN wafer, the orientation of the poling requires to couple the radiation as transverse magnetic (TM). The waveguides are placed on a 0.6 μm silicon dioxide (SiO_2) layer, bonded through a 0.2 μm gold (Au) layer to a silicon (Si) wafer (see Fig. 1(a)). The spatial distribution of the fundamental TM_{00} mode in the wavelength ranges of λ_p = 1 - 1.1 μm, λ_s = 1.53 - 1.57 μm and λ_i = 2.7 - 4 μm, their respective effective refractive indices and effective areas were obtained through numerical simulations based on a commercial software (MODE Solutions from ANSYS Inc.). The mode field diameters (MFDs) simulated at λ_p = 1 μm and λ_s = 1.55 μm were 6.248 μm and 6.303 μm, respectively, thus providing a very good mode matching with the fundamental mode of the optical fiber used for edge coupling (MFD = 6.6 μm @ 1 μm). From the numerical simulations performed at λ_i = 4 μm, it can be seen that the fundamental TM_{00} mode (see Fig. 1(b)) is very well confined in the LN ridge waveguide with a MFD of 6.631 μm and with a limited extent into the silica layer, thus limiting additional losses that might arise at MIR wavelengths due to the SiO_2 cladding material absorption. Addionally, it is worth noting that the mode size is weakly dependent on wavelength, resulting in an optimal spatial overlap between the three interacting wavelengths.

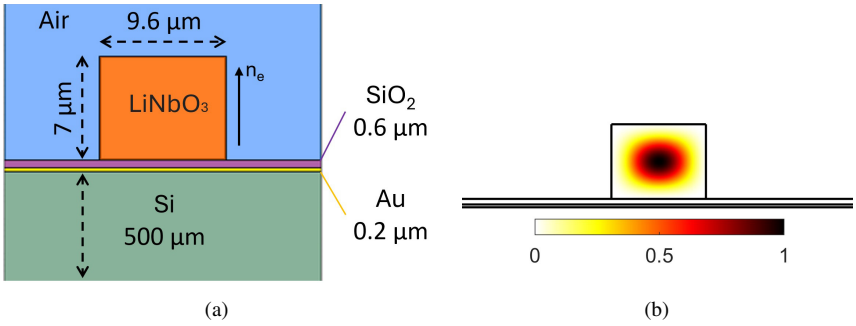

Fig. 1. (a) Cross-sectional view of the designed waveguide and dimensions. (b) Spatial distribution of the electric field of the fundamental TM_{00} mode numerically simulated at 4 μm.

The poling period was determined through numerical simulations to achieve quasi-phase matching across the desired wavelength range, with the results reported in Fig. 2(a). Figure 2(b) reports the phase-mismatch diagram that can be obtained considering a poling period equal to 25 μm. In this configuration, the phase-matching for the DFG nonlinear process can be preserved over a broad wavelength range from 2.7 to 3.5 μm by tuning the pump wavelength. By considering a LN waveguide with a different poling period, it is possible to shift the phase matching band to longer or shorter wavelengths.

The coupling efficiencies between a cleaved fiber (MFD = 6.6 μm @1 μm, as in the experiments) and the fundamental and higher-order TM modes of the designed LN waveguide were numerically calculated. The overall coupling efficiency was found to be equal to 80%, with most of the power

Optics EXPRESS

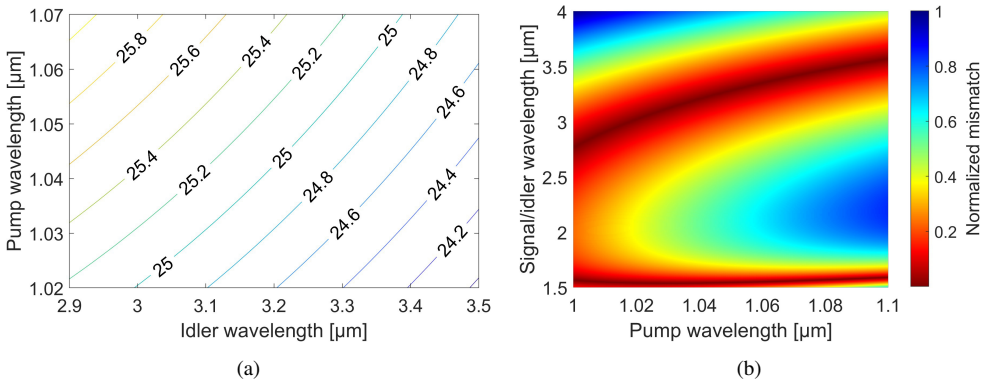

Fig. 2. (a) Numerical simulations of the required poling period (in µm) to satisfy the phase-matching condition as a function of the pump and idler wavelengths considering a signal wavelengths in the range 1530 - 70 nm. (b) Normalized phase mismatch diagram numerically simulated for a poling period equal to 25 µm.

coupled to only two modes: 73.2% of the total power was coupled into the TM_{00} mode and 6.2% was coupled into the TM_{02} mode. The maximum coupling to all the other modes was found to be negligible.

3. Fabrication

The first stage of the fabrication was to periodically pole a 500 µm thick, 4 inches diameter commercial z-cut congruent $LiNbO_3$ wafer by a standard technique involving the application of an intense electric field at room temperature [20] using a photo-resist pattern [Fig. 3(a)]. Several poling periods near 25 µm were inserted in the mask and realized to keep into account fabrication variations. In a subsequent stage, a SiO_2 layer was deposited by ICPECVD (Inductively-Coupled Plasma-Enhanced Chemical Vapour Deposition) onto one face of the poled wafer followed by the sputtering of a 100 nm-thick gold layer [Fig. 3(b)]. A high-flatness silicon wafer was also coated with a 100 nm-thick gold layer. The metallized faces of both the PPLN and silicon wafers were then placed into contact and pressed in a wafer bonding machine [Fig. 3(c)]. This metal diffusion bonding process was realized at room temperature which prevents mechanical stress that could occur due to the dissimilar temperature coefficients of the two wafers. The bonding procedure was completed by applying a strong pressure to the stack which yields more than 98% of the surface bonded, as observed by an ultrasound characterization technique. At the end of the process, a 1 mm thick hybrid structure composed of a silicon substrate bonded to a PPLN wafer is obtained. The structure was mechanically polished to obtain a 7 µm thick PPLN layer [Fig. 3(d)]. Note that this method was used earlier to produce adhered non-linear ridge waveguides [21–23] where either epoxy glue or direct bonding was used to fix the PPLN wafers onto $LiNbO_3$ or $LiTaO_3$ substrates. At this stage, the layers' thickness was examined to select the most homogeneous areas on the wafer. In the next step, two parallel trenches were cut in the PPLN layer by a precision dicing saw to form the lateral sides of the ridge waveguide [Fig. 3(e)]. The dicing parameters were set to minimize the roughness of the cut surfaces [24,25]. Finally, the hybrid wafer was diced to achieve polished input and output faces for the ridge waveguides.

Optics EXPRESS

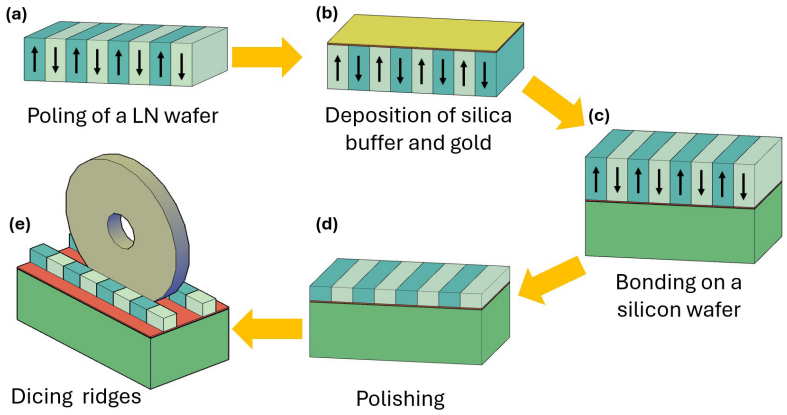

Fig. 3. Fabrication schematic: (a) periodically poling of a $LiNbO_3$ wafer; (b) deposition of silica and sputtering of gold buffer; (c) bonding of the PPLN wafer on a silicon wafer; (d) grinding and polishing of the PPLN side to reach the desired thickness; (e) dicing of the ridge waveguides and of the hybrid wafer.

4. Experimental setup

A schematic of the experimental setup used for the device characterization is reported in Fig. 4. It consists of a fiberized input side to couple the optical pump and signal into the PPLN waveguide and a free-space detection side to collect the output beams.

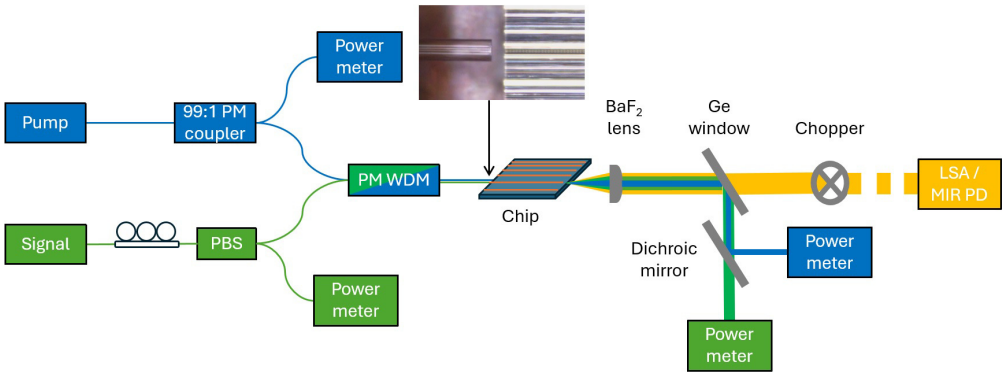

Fig. 4. Experimental setup used for the nonlinear DFG experiments. The photo shows the edge-coupling between a cleaved optical fiber and a PPLN waveguide. PBS: polarization beam splitter, PM WDM: polarization-maintaining wavelength division multiplexer, PM coupler: polarization-maintaining coupler, LSA: laser spectrum analyser, MIR PD: MIR photodiode. The fiberized/free-space blue, green and orange lines indicate the paths of the pump, signal and idler beams, respectively.

A custom-made CW tuneable laser source, able to generate Watt-level optical power in the wavelength band 1020 - 1065 nm, was employed as the optical pump. The laser consists of an oscillator with 6 mW maximum output power amplified through a co-propagating amplification stage. The oscillator's active medium is a Yb-doped polarization-maintaining (PM) optical fiber pumped with a 300 mW laser diode at 976 nm. The emission wavelength is set with a 1200-lines/mm grating mirror. The output of the oscillator, from a fiber coupler, is sent through a pump combiner to a double-clad Yb-doped PM amplifier pumped by a 10-W single-emitter

Optics EXPRESS

multimode laser diode at 915 nm. The amplified output is separated from the residual pump by a dichroic mirror and an isolator is added to avoid back reflections into the oscillator. A $\lambda/2$ waveplate and a C-coated lens are used to couple the laser output radiation in a PM optical fiber, which is then connected to a 99:1 PM fiber coupler. The power of the pump laser is monitored through a power meter that detects the 1% output of the 99/1 PM fiber coupler. The signal beam is generated by a CW laser (hp8168F) tuneable in the S-C bands, with a 100 kHz linewidth and 0.035 nm tuning accuracy. The signal is then amplified using an Erbium-doped fiber amplifier (EDFA) with maximum output power of 1W. Since the laser and the EDFA are not PM devices, a manual fiber polarization controller and a fiber polarization beam splitter (PBS) are used to precisely control the polarization of the signal coupled into the PPLN waveguide. The PBS limits the maximum signal power to around 500 mW. The polarization extinction is controlled by monitoring the power on one output of the PBS using a power meter. The pump and signal are combined together with a PM wavelength division multiplexer (WDM). The light is coupled into the PPLN waveguides through edge-coupling using a cleaved PM fiber (fiber PM980-XP), whose angle is controlled using a fiber rotator to excite the fundamental TM_{00} mode of the waveguide. The chip is mounted on a metal support equipped with a Peltier cell which can be used to change the temperature.

In the edge-coupling procedure, the spatial modes at the optical pump wavelength at the chip output facet were imaged using a CCD camera (Thorlabs DC1545M-G1) to maximize the power coupled into the TM_{00} mode of the waveguide. A free-space coupling scheme is set up to collect the output radiation from the chip using a BaF_2 lens with an anti-reflective coating between 2 - 5 μm to initially collimate the output light. The different wavelength components of the collimated output beam are split using a germanium (Ge) window with an anti-reflective coating between 1.9 - 6 μm and a dichroic mirror. The pump and signal beams are measured using two power meters (Ophir 3A-SH and Thorlabs PM16-122, respectively). The MIR beam component is modulated using a chopper and it is then measured initially through a laser spectrum analyser (BRISTOL 771-B MIR) to determine the wavelength of the generated idler and then using an InAsSb photodiode (Thorlabs PDA07P2) to retrieve the MIR power at the correspodning idler wavelengths. The modulated signal from the InAsSb photodiode is finally acquired through a USB oscilloscope (Digilent Analog Discovery 2).

5. Waveguide characterization

A linear characterization of the waveguides was initially carried out by measuring the waveguide propagation losses using the Fabry-Perot interferometric method, utilizing both fringe contrast and Fourier analysis [26]. We measured propagation losses in the S- and C-bands of ≈ 0.026 dB/cm. The coupling losses were also evaluated and we measured coupling efficiency of $\approx 75\%$ using a simple 90°-cleaved optical fiber, in good agreement with numerical simulations. These results highlight the advantages of using large waveguides compared to commonly used thin-film LN (TFLN) waveguides, both in terms of propagation and coupling losses. In particular, the high coupling efficiency was achieved without the use of lensed optical fibers thanks to the similar MFD of the PPLN waveguide and the single-mode fiber, thus providing even better long-term power stability in the experiments thanks to the relaxed tolerance in terms of fiber misalignment.

Nonlinear experiments were then carried out on a 3 cm-long PPLN waveguide with a poling period of 24.6 μm, and side dimensions of 7×9.6 μm^2.

The overall conversion bandwidth was evaluated by varying the pump wavelength λ_p at 5 nm steps from 1020 to 1065 nm. The signal wavelength λ_s was fine-tuned across the EDFA amplification spectrum for each λ_p value. The results of this characterization are reported in Fig. 5(a) (note that values indicated in the figure are normalized and refer to absolute MIR power values between 220 and 300 μW that are dependent on the pump power availability at the specific wavelength of operation). As expected from numerical simulations, we observed

Optics EXPRESS

that the maximum efficiency of the DFG process remains almost constant over a wide band in the MIR, approximately 460 nm. By finely tuning the wavelengths of both the pump and signal, it is possible to achieve the maximum efficiency for any desired MIR wavelength within this bandwidth. According to numerical simulations, using laser sources for the pump and signal with a broader tuneability, the range of the generated idler wavelengths could be further enlarged. The recorded peak normalized efficiency is equal to 3.24 %/W/cm^2, while the simulated one is equal to 6.73 %/W/cm^2. The efficiency is normalized by accounting for C-band losses and the nonlinear effective length of the waveguide, as in Ref. [15]. The nonlinear effective length of the waveguide accounts for the length of the waveguide over which the phase-matching condition can be considered actually satisfied and an effective nonlinear process takes place. This was evaluated by fixing the wavelength of the pump and varying the wavelength of the signal to retrieve the signal-conversion bandwidth. By comparing the measured full width at half maximum (FWHM) to the simulated one, an effective length of ≈ 70% of the total waveguide length was found. The reason behind this could be variations in the size and poling period along the waveguide. The difference between simulated and experimentally measured efficiencies could be likely attributed to higher MIR losses compared to the C-band losses and also to the limited nonlinear effective length of the waveguide. Through a comparison between experimental and simulated efficiencies, it is also possible to determine the maximum value of the loss in the MIR being equal to 1.5 dB/cm, by setting a nonlinear effective length equal to 70% of the real waveguide length.

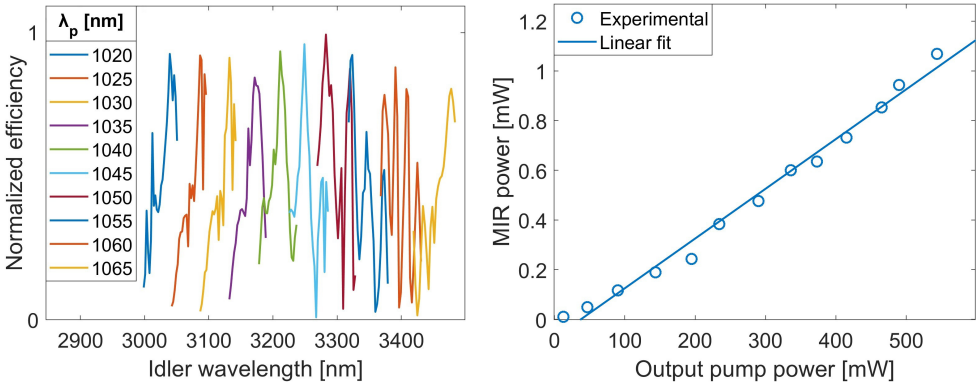

Fig. 5. (a) Normalized conversion efficiency as a function of the idler wavelength for different wavelengths of the pump source. (b) Idler output power as a function of the output pump power. The input signal power is fixed at 0.5 W; the wavelengths are set as: λ_p = 1040 nm, λ_s = 1537.8 nm and λ_i = 3212.76 nm.

To evaluate the idler output power as a function of the pump power, we set the pump wavelength λ_p = 1040 nm, the signal wavelength λ_s = 1537.8 nm with an EDFA output power P_s = 0.5 W and we continuously varied the pump power, recording the idler output power at λ_i = 3212.76 nm. The results are reported in Fig. 5(b). The output idler power grows linearly with the pump power up to the mW level, which satisfies the typical power requirements for direct absorption spectroscopy (DAS). DAS is one of the simplest methods for trace gas analysis and consists of the detection of a residual MIR beam that has propagated through a gas sample. The typically minimum required power for nearly shot-noise-limited MIR detection is of the order of 0.1 mW, depending on the detector [27]. Due to the input pump power limit in this test, we did not reach the saturation point of the conversion that we analytically estimated would be reached with a pump power in excess of 20 W, nor the damage threshold of the waveguide. By considering a similar waveguide structure [28], we estimate that the maximum power we could tolerate inside

Optics EXPRESS

the waveguide before reaching the damage threshold is 4 W (CW regime), occurring considerably sooner than the pump depletion-induced saturation point. Therefore, we can assume that is possible to generate even higher MIR optical power with the proposed device.

6. Conclusion

In conclusion, we discussed the design, fabrication and characteritazion of a PPLN waveguide for broadband, mW-level, NIR to MIR wavelength conversion. The generated MIR light was tuned by changing the wavelength of a 1.02 - 1.065 μm pump and a telecom C-band signal. Compared to conventional TFLN waveguides on silica devices [15], the here-proposed waveguide configuration benefits from a larger cross-section to achieve better mode confinement and lower propagation and coupling losses, thus allowing higher optical power levels for the generated idler. The demonstrated broadband fine-tuning in the ≈ 3 - 3.5 μm wavelength range, achievable output power level and the capability of translating the mature telecom technology in the MIR can be exploited for spectroscopy applications. Higher powers and broader conversion bands may be demonstrated in the future by improving the input laser sources and changing the chip temperature. Further progress in the realization of the poling mask may also enable the exploitation of the entire length of the waveguide for the DFG nonlinear process, increasing both efficiency and achievable output power.

Funding. H2020 Public-public partnerships (4R4R-IPP-20210405); Agence Nationale de la Recherche (ANR-23-PEEL-0004); European Union - NextGenerationEU, Mission 4 Component 1.5 (ECS00000036, CUP F17G22000190007).

Acknowledgments. We acknowledge the support of the French RENATECH network through its FEMTO-ST technological facility and funding by the European Union - NextGenerationEU, Mission 4 Component 1.5 - ECS00000036 - CUP F17G22000190007.

Disclosures. The authors declare no conflicts of interest.

Data availability. Data underlying the results presented in this paper are not publicly available at this time but may be obtained from the authors upon reasonable request.

References

1. U. Willer, M. Saraji, A. Khorsandi, *et al.*, "Near- and mid-infrared laser monitoring of industrial processes, environment and security applications," Optics and Lasers in Engineering **44**(7), 699–710 (2006).
2. M. V. Reboucas, J. B. dos Santos, D. Domingos, *et al.*, "Near-infrared spectroscopic prediction of chemical composition of a series of petrochemical process streams for aromatics production," Vib. Spectrosc. **52**(1), 97–102 (2010).
3. L. DRS, "MIRcat^{TM} Mid-IR Laser: Tune 1000 cm-1 at 1000s cm-1/s | High-Speed Tuning — daylightsolutions.com," https://www.daylightsolutions.com/products/mircat/ (2024). 07/19/2024.
4. Q. Lu, D. Wu, S. Sengupta, *et al.*, "Room temperature continuous wave, monolithic tunable THz sources based on highly efficient mid-infrared quantum cascade lasers," Sci. Rep. **6**(1), 23595 (2016).
5. F. Xie, C. Caneau, H. LeBlanc, *et al.*, "Room Temperature CW Operation of Short Wavelength Quantum Cascade Lasers Made of Strain Balanced GaxIn1-xAs/AlyIn1-yAs Material on InP substrates," IEEE J. SEL. TOP. QUANTUM ELECTR. **17**(5), 1445–1452 (2011).
6. I. Vurgaftman, R. Weih, M. Kamp, *et al.*, "Interband cascade lasers," J. Phys. D: Appl. Phys. **48**(12), 123001 (2015).
7. W. W. Bewley, C. L. Canedy, C. S. Kim, *et al.*, "High-power room-temperature continuous-wave mid-infrared interband cascade lasers," Opt. Express **20**(19), 20894–20901 (2012).
8. W. Geng, Y. Fang, Y. Wang, *et al.*, "Nonlinear photonics on integrated platforms," Nanophotonics **13**(18), 3253–3278 (2024).
9. V. Vitali, I. Demirtzioglou, C. Lacava, *et al.*, "Nonlinear signal processing on chip," in *On-Chip Photonics* (Elsevier, 2024), pp. 273–296.
10. D. Zhu, L. Shao, M. Yu, *et al.*, "Integrated photonics on thin-film lithium niobate," Adv. Opt. Photonics **13**(2), 242–352 (2021).
11. B. You, S. Yuan, Y. Tian, *et al.*, "Lithium niobate on insulator – fundamental opto-electronic properties and photonic device prospects," Nanophotonics **13**(17), 3037–3057 (2024).
12. Y. Qi and Y. Li, "Integrated lithium niobate photonics," Nanophotonics **9**(6), 1287–1320 (2020).
13. M. Xu, M. He, H. Zhang, *et al.*, "High-performance coherent optical modulators based on thin-film lithium niobate platform," Nat. Commun. **11**(1), 3911 (2020).
14. D. Pohl, M. Reig Escalé, M. Madi, *et al.*, "An integrated broadband spectrometer on thin-film lithium niobate," Nat. Photonics **14**(1), 24–29 (2020).

Optics EXPRESS

15. J. Mishra, T. P. McKenna, E. Ng, *et al.*, "Mid-infrared nonlinear optics in thin-film lithium niobate on sapphire," in *Conference on Lasers and Electro-Optics* (2021), pp. 1–2.
16. S. Liang, Y. Jung, K. R. H. Bottrill, *et al.*, "L-band Mode and Wavelength Conversion in a Periodically Poled Lithium Niobate Ridge Waveguide," in *European Conference on Optical Communication* (Optica Publishing Group, 2022), paper Tu5.22.
17. J. Mishra, M. Jankowski, A. Y. Hwang, *et al.*, "Ultra-broadband mid-infrared generation in dispersion-engineered thin-film lithium niobate," Opt. Express **30**(18), 32752–32760 (2022).
18. C. Hu, A. Pan, T. Li, *et al.*, "High-efficient coupler for thin-film lithium niobate waveguide devices," Opt. Express **29**(4), 5397–5406 (2021).
19. L. Deng, X. Gao, Z. Cao, *et al.*, "Improvement to Sellmeier equation for periodically poled LiNbO3 crystal using mid-infrared difference-frequency generation," Opt. Commun. **268**(1), 110–114 (2006).
20. E. Courjon, N. Courjal, W. Daniau, *et al.*, "Lamb wave transducers built on periodically poled Z-cut LiNbO3 wafers," J. Appl. Phys. **102**(11), 114107 (2007).
21. R. Kou, S. Kurimura, K. Kikuchi, *et al.*, "High-gain, wide-dynamic-range parametric interaction in Mg-doped LiNbO3 quasi-phase-matched adhered ridge waveguide," Opt. Express **19**(12), 11867–11872 (2011).
22. S. Kurimura, Y. Kato, M. Maruyama, *et al.*, "Quasi-phase-matched adhered ridge waveguide in LiNbO3," Appl. Phys. Lett. **89**(19), 191123 (2006).
23. M. Chauvet, F. Henrot, F. Bassignot, *et al.*, "High efficiency frequency doubling in fully diced LiNbO 3 ridge waveguides on silicon," J. Opt. **18**(8), 085503 (2016).
24. M. F. Volk, S. Suntsov, C. E. Rüter, *et al.*, "Low loss ridge waveguides in lithium niobate thin films by optical grade diamond blade dicing," Opt. Express **24**(2), 1386–1391 (2016).
25. N. Courjal, B. Guichardaz, G. Ulliac, *et al.*, "High aspect ratio lithium niobate ridge waveguides fabricated by optical grade dicing," J. Phys. D: Appl. Phys. **44**(30), 305101 (2011).
26. D. Hofstetter and R. L. Thornton, "Theory of loss measurements of Fabry–Perot resonators by Fourier analysis of the transmission spectra," Opt. Lett. **22**(24), 1831–1833 (1997).
27. M. Vainio and L. Halonen, "Mid-infrared optical parametric oscillators and frequency combs for molecular spectroscopy," Phys. Chem. Chem. Phys. **18**(6), 4266–4294 (2016).
28. V. Pecheur, H. Porte, J. Hauden, *et al.*, "Watt-level SHG in undoped high step-index PPLN ridge waveguides," OSA Continuum **4**(5), 1404–1414 (2021).